

# Big-Bang Nucleosynthesis and Gravitino

<sup>(a)(b)</sup>Masahiro Kawasaki, <sup>(c)</sup>Kazunori Kohri, <sup>(d)</sup>Takeo Moroi,  
<sup>(d)</sup>Akira Yotsuyanagi

<sup>(a)</sup>*Institute for Cosmic Ray Research, University of Tokyo, Kashiwa 277-8582, JAPAN*

<sup>(b)</sup>*Institute for the Physics and Mathematics of the Universe, University of Tokyo,  
Kashiwa 277-8582, JAPAN*

<sup>(c)</sup>*Physics Department, Lancaster University, Lancaster LA1 4YB, UK*

<sup>(d)</sup>*Department of Physics, Tohoku University, Sendai 980-8578, JAPAN*

## Abstract

We derive big-bang nucleosynthesis (BBN) constraints on both unstable and stable gravitino taking account of recent progresses in theoretical study of the BBN processes as well as observations of primordial light-element abundances. In the case of unstable gravitino, we set the upper limit on the reheating temperature assuming that the primordial gravitinos are mainly produced by the scattering processes of thermal particles. For stable gravitino, we consider Bino, stau and sneutrino as the next-to-the-lightest supersymmetric particle and obtain constraints on their properties. Compared with the previous works, we improved the following points: (i) we use the most recent observational data, (ii) for gravitino production, we include contribution of the longitudinal component, and (iii) for the case with unstable long-lived stau, we estimate the bound-state effect of stau accurately by solving the Boltzmann equation.

# 1 Introduction

It is well known that, in the framework of the standard model of particle physics, viable scenario of the evolution of the universe cannot be obtained. One of the most important reasons is that, in the standard model, there is no candidate of dark matter. Among various possibilities, the lightest superparticle (LSP) in supersymmetric models is a good candidate of dark matter, and hence supersymmetry is thought to be very attractive from the cosmological point of view as well as from particle-physics point of view.

In considering cosmology based on supersymmetric models with  $R$ -parity conservation, it is important to be aware that graviton also has its superpartner, which is called gravitino. Even though gravitino is an extremely weakly interacting particle, it may play a significant role in the evolution of the universe. In particular, with the existence of gravitino, there may exist a long-lived superparticle whose lifetime is longer than  $\sim 0.1$  sec. For example, if one of the superparticles of standard-model particles is the LSP, gravitino becomes unstable and is very long-lived. On the contrary, if the gravitino is the LSP, lightest superparticle in the minimal supersymmetric standard model (MSSM) sector, which we call MSSM-LSP, decays into gravitino (and something else) with a Planck-scale suppressed decay width.

Long-lived superparticles may affect the big-bang nucleosynthesis (BBN) if their lifetimes are longer than  $\sim 0.1$  sec. Such a long-lived superparticle is produced in the early universe and decays in the thermal bath at the cosmic time comparable to its lifetime. Importantly, the energetic particles emitted by the decay may induce hadronic and electromagnetic shower and produce large amount of energetic hadrons and/or photons. Those energetic hadrons and photons induce hadro- and photo-dissociation processes of light elements which are synthesized by the standard BBN (SBBN) reactions. In addition, mesons such as charged pions are also produced in the hadronic shower induced by the decay of long-lived particle. Such charged pions and baryons cause extraordinary  $p \leftrightarrow n$  conversion processes, resulting in the change of  ${}^4\text{He}$  abundance. Since the predictions of the SBBN scenario are in reasonable agreements with observations, we obtain upper bound on the primordial abundance of the long-lived superparticle.

In this paper, we study the BBN scenario in detail for the cases where gravitino is unstable and stable, and derive constraints on those cases. In supersymmetric model, such BBN constraints have been extensively studied for the cases where gravitino is unstable [1, 2, 3, 4, 5, 6, 7, 8] and stable [9, 10, 11, 12, 13]. The primary purpose of this paper is to study the constraints on scenarios with long-lived superparticles from the BBN scenario, taking account of recent developments in this field. Compared to the most recent studies [5, 6, 7, 13, 14], we have improved the following points:

- We have used the most recent observational constraints on the primordial abundances of light elements.
- We have taken into account the contribution of the production of the longitudinal component of gravitino in the calculation of the primordial abundance of gravitino.

Consequently, we have obtained severer upper bound on the reheating temperature for the case of unstable gravitino, in particular when the gravitino mass is relatively light.

- For the case that the gravitino is the LSP and a charged slepton is the next-to-lightest supersymmetric particle (NLSP), we have calculated the abundance of the bound state of the charged slepton with  ${}^4\text{He}$  solving the Boltzmann equation without the use of Saha formula and hence have estimated the catalyzed production of  ${}^6\text{Li}$  precisely. In addition, for the scenario with Bino-like NLSP, we have performed a detailed analysis.

The organization of this paper is as follows. In Section 2, we first summarize how the BBN processes are analyzed taking into account the effects of long-lived superparticles. Then, in Section 3, we discuss constraints on the case where gravitino is unstable. We pay particular attention to the scenario where the LSP is the lightest neutralino and derive the upper bound on the reheating temperature after inflation. In Section 4, we consider the case where gravitino is the LSP and hence is stable. In such a case, the MSSM-LSP becomes unstable and its decay may affect the BBN scenario. The constraints depends on what the MSSM-LSP is, so we consider several cases where the MSSM-LSP is the lightest neutralino, one of the charged slepton, and one of the sneutrino. Section 5 is devoted to conclusions and discussion.

## 2 BBN with Long-Lived Unstable Particles

### 2.1 Effects of the long-lived particle and calculation procedure

We first summarize the general procedure to study effects of long-lived unstable particles on BBN. In particular, in this section, we explain how we calculate non-standard BBN reaction rates with long-lived unstable particles. We also summarize observational constraints on light-element abundances which will be adopted in our study.

In our study, we consider two important types of decay modes of long-lived particles: radiative decay and hadronic decay. With the radiative decay, photon and/or charged particles are emitted. Then the light elements would be photo-disintegrated (or photo-dissociated) by energetic photons which are produced in the electro-magnetic shower induced by high energy photons/charged particles [2, 3, 4, 8, 15]. With the hadronic decay, the emitted hadrons induce extraordinary interconversions between background proton and neutron ( $p \leftrightarrow n$  conversion) through the strong interaction. Such conversion processes enhance the neutron-to-proton ratio, resulting in the over-production of  ${}^4\text{He}$  [16, 5, 6, 7, 17]. The energetic nucleons also destroy the background  ${}^4\text{He}$  and nonthermally produce other light elements, such as D, T,  ${}^3\text{He}$ ,  ${}^6\text{Li}$ ,  ${}^7\text{Li}$  and  ${}^7\text{Be}$  [18, 19, 5, 6, 7, 17]. Furthermore, if the long-lived particle is charged, it may form a bound state with background nuclei and change the nuclear reaction rates. In particular, for the production of  ${}^6\text{Li}$ , such a process, which is called catalyzed production process [20], may become very important.

We incorporate these effects, photo-dissociation,  $p \leftrightarrow n$  conversion, hadro-dissociation, and catalyzed production process for the case with charged long-lived particle, into a stan-

standard BBN code [21] and calculate light-element abundances. (Some details of these effects are discussed in the following.) In order to estimate errors in theoretical calculation, we perform Monte-Carlo simulation by changing both the standard and non-standard reaction rates within their statistical and systematic errors. (For the baryon-to-photon ratio, we use  $\eta = 6.10 \pm 0.21$  [22].) The estimated errors in the calculation of light-element abundances are used in the estimation of the  $\chi^2$  variable to derive BBN constraints; in the calculation of the  $\chi^2$  variable, theoretical and observational errors are added in quadrature.

### 2.1.1 Radiative decay

In order to study the effects of radiative decay, we numerically solve the Boltzmann equation governing the time evolution of the photon and electron spectra. To obtain photo-dissociation rates, we take convolutions of the photon spectrum and the energy-dependent cross sections. In the following, we briefly discuss our treatment of the photo-dissociation processes. (For the details of the effects of radiative decay, see [3].)

If the parent particle radiatively decays into high-energy photons or charged particles, those daughter particles scatter off the background photons  $\gamma_{\text{BG}}$  and electrons  $e_{\text{BG}}^-$  via electromagnetic interaction. (Here, the subscript “BG” is for background particles in the thermal bath.) The most important processes are the Compton scattering ( $\gamma + e_{\text{BG}}^- \rightarrow \gamma + e^-$ ), the electron-positron pair creation ( $\gamma + \gamma_{\text{BG}} \rightarrow e^- + e^+$ ), the pair creation in nuclei ( $\gamma + N \rightarrow e^- + e^+ + N$ , with  $N$  being the background nuclei), the photon-photon scattering ( $\gamma + \gamma_{\text{BG}} \rightarrow \gamma + \gamma$ ), and the inverse Compton scattering ( $e^- + \gamma_{\text{BG}} \rightarrow e^- + \gamma$ ). Consequently, the electromagnetic cascade shower is induced and a series of these processes produce many photons.

The timescale of the energy loss processes of the photons is much faster than the timescale of cosmic expansion if the cosmic temperature is sufficiently high  $T > O(1 \text{ eV})$ . On the other hand, the thermalization timescale of the photons can be longer than that to react with the background light elements, and hence the photons may cause the photo-dissociation processes; the photo-dissociation process with the threshold energy of  $Q$  becomes effective when the cosmic temperature is lower than  $\sim m_e^2/22Q$  [4]. For the photo-dissociation of D ( $^4\text{He}$ ), for which the threshold energy is  $Q \sim 2.2\text{keV}$  (20 MeV), the cosmic temperature should be lower than  $\sim 10\text{keV}$  ( $\sim 1\text{keV}$ ).

In addition, once the  $^4\text{He}$  is destructed, energetic T and  $^3\text{He}$  are produced. They scatter off background  $^4\text{He}$  and produce  $^6\text{Li}$  nonthermally. We also include photo-dissociation processes of  $^6\text{Li}$ ,  $^7\text{Li}$  and  $^7\text{Be}$ .

### 2.1.2 Hadronic decay

Next, we summarize how the effects of hadronic decay are studied. If the parent particle decays into quarks and/or gluons, they immediately fragment into high-energy hadrons. Comparing the lifetime of the produced hadrons with the timescale of their interactions with the background nuclei, only long-lived mesons,  $\pi^\pm$ ,  $K^\pm$ ,  $K_L^0$ , as well as the nucleons

$n$  and  $p$  are important for the study of the BBN reactions; hadrons with shorter lifetimes decay before scattering off the background nuclei.

We calculate the distributions of partons emitted from the decaying parent particle. In particular, for the systematic study of the decay chain, we use the ISAJET/ISASUSY packages [23]. Then fragmentation processes of the partons into hadrons are simulated by using the event generator PYTHIA [24] and finally the distributions of the produced hadrons are obtained.

The long-lived (and stable) hadrons destroy the background  ${}^4\text{He}$  and produce D, T, and  ${}^3\text{He}$  copiously. Furthermore, the energetic daughter T,  ${}^3\text{He}$  and the scattered  ${}^4\text{He}$  also nonthermally produce  ${}^6\text{Li}$ ,  ${}^7\text{Li}$  and  ${}^7\text{Be}$  through the collisions with the background  ${}^4\text{He}$ . These processes are severely constrained by the observations [19, 5, 6].

On the other hand, the neutron injection at around  $T \sim 30$  keV may reduce the final abundance of  ${}^7\text{Be}$  (or  ${}^7\text{Li}$ ) through the neutron capture process,  ${}^7\text{Be}(n,p){}^7\text{Li}(p,\alpha){}^4\text{He}$  [25, 6, 7, 12, 26]. However, this process does not affect our constraints because we adopt a very mild observational abundance of  ${}^7\text{Li}$ .

With the hadronic decay, the conversion processes of the background  $p$  and  $n$  also occur. In particular, once protons, neutrons, and pions (and their anti-particles) are produced in the hadronic shower, they induce  $p \leftrightarrow n$  conversion processes and change the neutron to proton ratio  $n/p$  even after the normal freeze-out epoch of neutron.<sup>#1</sup> Such  $p \leftrightarrow n$  conversion processes increase  ${}^4\text{He}$  and hence are constrained from observation of the primordial abundance of  ${}^4\text{He}$ .

We solve the time-evolution of the hadron distribution functions including all the relevant electromagnetic and hadronic energy-loss processes, and calculate the reaction rates of the light elements taking into account the hadro-dissociation and  $p \leftrightarrow n$  conversion processes (as well as those of the photo-dissociation). For further details, readers can refer to [6].

Before closing this subsection, we discuss the minor modification of the treatment of the hadronic shower compared to the previous studies [5, 6, 7]. In the present study, we adopted a new evolution scheme of the hadronic shower. For the study of the abundance of non-thermally produced  ${}^6\text{Li}$ ,  ${}^7\text{Li}$  and  ${}^7\text{Be}$ , it is important to obtain information on the energy distribution of  ${}^4\text{He}$  produced by the scattering process  $N + {}^4\text{He} \rightarrow N' + {}^4\text{He} + \pi$ . However, there is a lack of experimental data of the energy distribution of the scattered  ${}^4\text{He}$  in the inelastic  $N + {}^4\text{He}$  collision. In the old papers [5, 6, 7], quantum chromodynamics (QCD) properties was used to extrapolate results of high-energy experiments to lower energies (as far as the extrapolation is kinematically allowed). Consequently, the final-state  ${}^4\text{He}$  acquired larger energy than that estimated via equipartition distribution in the center-of-mass system. However, in the present study, we adopted the smaller value of the  ${}^4\text{He}$  energy among the equipartition value and the QCD prediction. This procedure gives more conservative constraints. For non-relativistic  $N + {}^4\text{He}$  collisions, this modified method gives smaller energies of the scattered  ${}^4\text{He}$ , which reduces the resultant nonthermally produced Li and Be by  $\sim 50$  % or so [26]. However, this does not affect the constraints given in [5, 6, 7]. That

---

<sup>#1</sup>We omit contributions from  $K^\pm$  and  $K_L^0$  to this  $p \leftrightarrow n$  conversion according to a discussion in [6] although there have been some attempts to include effects of Kaons [16, 5].

is because the nonthermally produced Li and Be are subdominant compared to the SBBN contributions, and also because we adopt conservative observational constraints.

## 2.2 Observational light-element abundances

Next, we show observational constants on primordial abundances of D,  $^3\text{He}$ ,  $^4\text{He}$ ,  $^6\text{Li}$  and  $^7\text{Li}$ , which we adopt in our study. The errors are presented at  $1\sigma$ . The subscript “p” and “obs” are for the primordial and observational values, respectively.

We adopt the following observational constraints on the deuterium abundance

$$(n_{\text{D}}/n_{\text{H}})_{\text{p}} = (2.82 \pm 0.26) \times 10^{-5}, \quad (2.1)$$

which is the most-recently reported value of the weighted mean [27]. This value well agrees with the baryon to photon ratio suggested by the WMAP 3-year CMB anisotropy observation [22].

To constrain the primordial  $^3\text{He}$  abundance, we use an observational  $^3\text{He}$  to D ratio as an upper bound, which is a monotonically increasing function of the cosmic time. (For details, see [28, 5, 6].) In this study we adopt the newest values of D and  $^3\text{He}$  abundances simultaneously observed in protosolar clouds (PSCs),  $(n_{^3\text{He}}/n_{\text{H}})_{\text{PSC}} = (1.66 \pm 0.06) \times 10^{-5}$  and  $(n_{\text{D}}/n_{\text{H}})_{\text{PSC}} = (2.00 \pm 0.35) \times 10^{-5}$  [29]. Then we get

$$(n_{^3\text{He}}/n_{\text{D}})_{\text{p}} < 0.83 + 0.27. \quad (2.2)$$

Concerning the mass fraction of  $^4\text{He}$ , in [30], two values are recently reported by using old and new  $^4\text{He}$ -emissivity data,  $Y_{\text{p}} = 0.2472 \pm 0.0012$  and  $Y_{\text{p}} = 0.2516 \pm 0.0011$ , respectively. It should be noted that the latter value is inconsistent with the SBBN prediction ( $\simeq 0.2484$ ) even adopting possible theoretical errors of 0.0004. However, we do not take its face value since the error presented in [30] does not include systematic effects. Thus, in this study, we add an error of 0.0040 [31] to derive conservative constraint:

$$Y_{\text{p}} = 0.2516 \pm 0.0040. \quad (2.3)$$

(For the systematic uncertainty of the observed  $^4\text{He}$  abundance, see also [32].)

For  $^7\text{Li}$ , we adopt the most recent value of the  $^7\text{Li}$  to hydrogen ratio  $\log_{10}(^7\text{Li}/\text{H})_{\text{obs}} = -9.90 \pm 0.09$  given in [33]. This is close to the value given in [34]:  $\log_{10}(^7\text{Li}/\text{H})_{\text{obs}} = -9.91 \pm 0.10$ , and in addition, slightly larger values have been also reported for years; for example, see [35]:  $\log_{10}(^7\text{Li}/\text{H})_{\text{obs}} = -9.63 \pm 0.06$ . Those observational values are smaller than the SBBN prediction by approximately 0.3 dex or so. Concerning the inconsistency between the face value of the primordial  $^7\text{Li}$  abundance and the SBBN prediction, various solutions have been discussed from the viewpoint of both astrophysics [36, 37] and cosmology [38, 25, 7, 12, 17, 39, 11, 40, 41, 26, 42, 43, 44]. However, the main purpose of this paper is to derive a conservative constraint, so we do not go into the details of these models. Instead, we add an additional systematic error of +0.3 dex into the observational face value  $n_{^7\text{Li}}/n_{\text{H}}$  in our study:

$$\log_{10}(n_{^7\text{Li}}/n_{\text{H}})_{\text{p}} = -9.90 \pm 0.09 + 0.3. \quad (2.4)$$

Notice that +0.3 dex is the systematic error expected from effect of  ${}^7\text{Li}$  depletion by rotational mixing in stars [36].<sup>#2</sup>

As for a  ${}^6\text{Li}$  constraint, we use  $(n_{6\text{Li}}/n_{7\text{Li}})_{\text{obs}} = 0.046 \pm 0.022$ , which was newly-observed in a very metal-poor star [47]. We also add a systematic error of +0.084 [13] to take into account depletion effects in stars adopting the relation between  ${}^7\text{Li}$  and  ${}^6\text{Li}$  depletion factors,  $\Delta \log_{10}(n_{6\text{Li}}/n_{\text{H}}) = 2.5\Delta \log_{10}(n_{7\text{Li}}/n_{\text{H}})$  [48, 36], which leads to  $\Delta \log_{10}(n_{6\text{Li}}/n_{7\text{Li}}) = 0.45$  with  ${}^7\text{Li}$  depletion factor 0.3 dex. Then we get the following upper bound:

$$(n_{6\text{Li}}/n_{7\text{Li}})_p < 0.046 \pm 0.022 + 0.084. \quad (2.5)$$

## 3 Unstable Gravitino

### 3.1 Primordial abundance of gravitino

When gravitino is unstable, gravitinos produced in the early universe may affect the light-element abundances because the lifetime of gravitino is extremely long. Indeed, if gravitino is lighter than  $\sim O(10 \text{ TeV})$ , its lifetime becomes longer than  $\sim 1\text{sec}$  and, in such a case, most of the primordial gravitinos decay after the BBN starts. Since the predictions of the SBBN are in reasonable agreements with observations, the abundance of gravitino is required to be small enough. Thus, we obtain upper bound on the abundance of primordial gravitino.

There are several possible mechanisms of producing gravitino in the early universe; gravitino may be from the decay of condensations of scalar fields, like moduli fields [49] or inflaton field [50], as well as from scattering processes of particles in the thermal bath. Gravitino production due to the decay of scalar condensations is, however, highly model-dependent. In order to derive conservative constraints, we presume that the primordial gravitinos originate from the scattering processes. In such a case, the abundance of gravitino is approximately proportional to the reheating temperature after inflation. Then, in order not to spoil the success of BBN scenario, upper bound on the reheating temperature is derived.

Concentrating on the gravitino production by the scattering, the evolution of the number density of gravitino is governed by the following Boltzmann equation:

$$\frac{dn_{3/2}}{dt} = -3Hn_{3/2} + C_{3/2}, \quad (3.1)$$

where  $H$  is the expansion rate of the universe and  $C_{3/2}$  is the collision term. In our analysis, we study the above Boltzmann equation simultaneously with other relevant equations:<sup>#3</sup>

$$\frac{d\rho_{\text{inf}}}{dt} = -3H\rho_{\text{inf}} - \Gamma_{\text{inf}}\rho_{\text{inf}}, \quad (3.2)$$

$$\frac{d\rho_{\text{rad}}}{dt} = -4H\rho_{\text{rad}} + \Gamma_{\text{inf}}\rho_{\text{inf}}, \quad (3.3)$$

---

<sup>#2</sup>See also [45, 46] for detailed discussion on possible systematic uncertainties.

<sup>#3</sup>Here, we assume that the potential of the inflaton field is well approximated by parabolic potential.

where  $\rho_{\text{inf}}$  and  $\rho_{\text{rad}}$  are energy densities of inflaton and radiation, respectively, and  $\Gamma_{\text{inf}}$  is the decay rate of the inflaton field. We numerically solve Eqs. (3.1) – (3.3) with initial conditions  $n_{3/2} = 0$  and  $\rho_{\text{inf}} \gg \rho_X$ ; we follow the evolution of  $n_{3/2}$ ,  $\rho_{\text{inf}}$ , and  $\rho_{\text{rad}}$  from the inflaton-dominated epoch (i.e.,  $t \ll \Gamma_{\text{inf}}^{-1}$ ) to the radiation-dominated epoch (i.e.,  $t \gg \Gamma_{\text{inf}}^{-1}$ ). Most of the energy density stored in the inflaton is converted to that of radiation at the reheating temperature which is of the order of  $\sqrt{M_* \Gamma_{\text{inf}}}$  (with  $M_* \simeq 2.4 \times 10^{18}$  GeV being the reduced Planck scale); in this paper, the reheating temperature is defined as  $3H(T_R) = \Gamma_{\text{inf}}$  which gives

$$T_R \equiv \left( \frac{10}{g_*(T_R)\pi^2} M_*^2 \Gamma_{\text{inf}}^2 \right)^{1/4}, \quad (3.4)$$

where  $g_*(T_R)$  is the effective number of the massless degrees of freedom at the time of reheating. In our study, we use  $g_*(T_R) = 228.75$ .

The collision term has been calculated in [51, 52] by taking account of the thermal masses for gauge-boson propagators:

$$C_{3/2} = \frac{\zeta(3)T^6}{16\pi^3 M_*^2} \sum_a c_a g_a^2(T) \left( 1 + \frac{M_a^2(T)}{3m_{3/2}^2} \right) \ln \frac{k_a}{g_a(T)}, \quad (3.5)$$

where the summation is over the standard-model gauge groups, and  $c_a = 11, 27$ , and  $72$ , while  $k_a = 1.266, 1.312$ , and  $1.271$ , for  $U(1)_Y$ ,  $SU(2)_L$ , and  $SU(3)_C$ , respectively.<sup>#4</sup> In addition,  $M_a$  ( $a = 1 - 3$ ) denotes the gaugino mass. Compared to the previous works on unstable gravitino [6, 7], we have included the production of the longitudinal mode, (part of) which is from the term proportional to  $M_a^2/m_{3/2}^2$  in Eq. (3.5). Although we numerically calculate the primordial abundance of gravitino, we also provide its fitting formula. Let us define the yield variable for particle  $X$  with lifetime  $\tau_X$  as

$$Y_X \equiv \left[ \frac{n_X}{s} \right]_{t \ll \tau_X}, \quad (3.6)$$

where  $n_X$  is the number density of  $X$  and  $s$  is the entropy density. Then, when the gaugino masses obey the grand-unified-theory (GUT) relation, the yield variable of gravitino is well fitted by

$$Y_{3/2} \simeq 2.3 \times 10^{-14} \times T_R^{(8)} \left[ 1 + 0.015 \ln T_R^{(8)} - 0.0009 \ln^2 T_R^{(8)} \right] \\ + 1.5 \times 10^{-14} \times \left( \frac{m_{1/2}}{m_{3/2}} \right)^2 T_R^{(8)} \left[ 1 - 0.037 \ln T_R^{(8)} + 0.0009 \ln^2 T_R^{(8)} \right], \quad (3.7)$$

where  $T_R^{(8)} \equiv T_R/10^8$  GeV and  $m_{1/2}$  is the unified gaugino mass at the GUT scale. The above fitting formula agrees well with the numerical result with the error of a few % for  $10^5 \text{ GeV} \leq T_R \leq 10^{12} \text{ GeV}$ .

---

<sup>#4</sup>See also [53] for possible corrections.



	Case 1	Case 2	Case 3	Case 4
$m_{1/2}$	300 GeV	600 GeV	300 GeV	1200 GeV
$m_0$	141 GeV	218 GeV	2397 GeV	800 GeV
$A_0$	0	0	0	0
$\tan \beta$	30	30	30	45
$\mu_H$	389 GeV	726 GeV	231 GeV	-1315 GeV
$m_{\chi_1^0}$	117 GeV	244 GeV	116 GeV	509 GeV
$\Omega_{\text{LSP}}^{(\text{thermal})} h^2$	0.111	0.110	0.106	0.111

Table 1: mSUGRA parameters used in our analysis.

## 3.2 Models

In order to study effects of photo- and hadro-dissociations and  $p \leftrightarrow n$  conversion, it is necessary to understand the energy spectra of daughter particles produced by the decay of gravitino. If gravitino is not the LSP, gravitino decays into a lighter superparticle and standard-model particle(s). Those daughter particles also decay if they are unstable. The decay chain strongly depends on the mass spectrum (and coupling constants) of the MSSM particles. Since there are so many parameters in the MSSM, it is difficult to consider the whole parameter space. Thus, we adopt four parameter points of the so-called mSUGRA model to fix the MSSM parameters. Then, for those parameter points, we calculate decay chain of the gravitino in details and derive BBN constraints.

In the mSUGRA model, all the MSSM parameters are determined by the unified gaugino mass  $m_{1/2}$ , universal scalar mass  $m_0$ , universal coefficient for the tri-linear scalar coupling  $A_0$ , ratio of the vacuum expectation values of two Higgs bosons  $\tan \beta$ , and supersymmetric Higgs mass  $\mu_H$ . ( $|\mu_H|$  is determined by the condition of electro-weak symmetry breaking.) The points we choose are shown in Table 1. For the points we choose, we also calculate the thermal relic density of the lightest neutralino, which is the LSP; the resultant density parameters are also shown in Table 1. (We use  $h = 0.73$  [22], where  $h$  is the expansion rate of the universe in units of 100 km/sec/Mpc.) Notice that the Cases 1 and 2 are in the so-called “co-annihilation region,” the Case 3 is in the “focus-point region,” and the Case 4 is in “Higgs funnel region.”

With the mSUGRA parameters given in Table 1, the mass spectrum of the MSSM particles as well as coupling parameters are obtained. Then, we calculate the decay rate of gravitino  $\Gamma_{3/2}$ , taking account of all the relevant decay modes. The lifetime of gravitino is given by  $\tau_{3/2} = \Gamma_{3/2}^{-1}$ ; we show the lifetime for each cases in Fig. 1. The lifetime depends on the mass spectrum of the MSSM particles when the gravitino mass is relatively light. When gravitino becomes very heavy, on the contrary,  $\tau_{3/2}$  is determined only by the number of possible decay modes. In the present case, as one can see in Fig. 1, the lifetime becomes insensitive to the mass spectrum of the final-state particles when  $m_{3/2} \gtrsim 10$  TeV.

The decay processes of the daughter particles from the gravitino decay are also important;

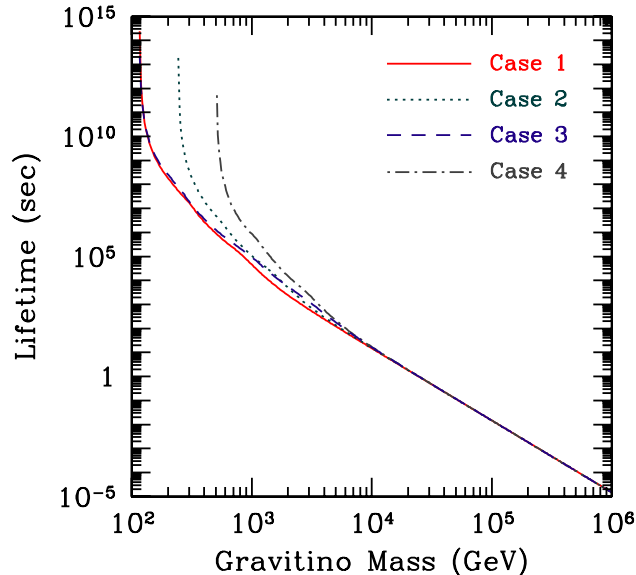


Figure 1: Lifetime of gravitino for Cases 1 – 4. The horizontal axis is the gravitino mass.

we also calculate partial decay rates of the unstable superparticles to follow the decay chain. The energy spectra of the decay products are obtained by using Monte-Carlo analysis. At the parton level, the decay chain induced by the gravitino decay is systematically followed by using ISAJET/ISASUSY packages [23], while the hadronization processes of partons are studied by using PYTHIA package [24]. Then, we obtain energy spectra of (quasi) stable particles for the study of the light-element abundances; once the spectra of hadronic particles (in particular, those of proton, neutron, and pions) as well as the averaged visible energy from the gravitino decay are obtained, we calculate light-element abundances taking account of photo- and hadro-dissociation processes as well as  $p \leftrightarrow n$  conversion processes.

### 3.3 Numerical results

We show our numerical results in Figs. 2 – 5 for Cases 1 – 4, respectively. These figures show upper bounds on the reheating temperature as functions of the gravitino mass. Since, in this section, we consider unstable gravitino, we shade the region where the gravitino becomes lighter than the MSSM-LSP and hence is stable. Solid lines show upper bounds on the reheating temperature from individual light elements; the upper-left regions are excluded at 95 % C.L. Compared with the previous work [7], we have newly included contributions of the production of the longitudinal component of gravitino. (See Eq. (3.7)). This modification gives us severer upper bounds on the reheating temperature when the gravitino is relatively light. Upper bound on the reheating temperature is summarized in Table 2 for several values of the gravitino mass .

When the gravitino is unstable, the LSP (i.e., the lightest neutralino in this case) is

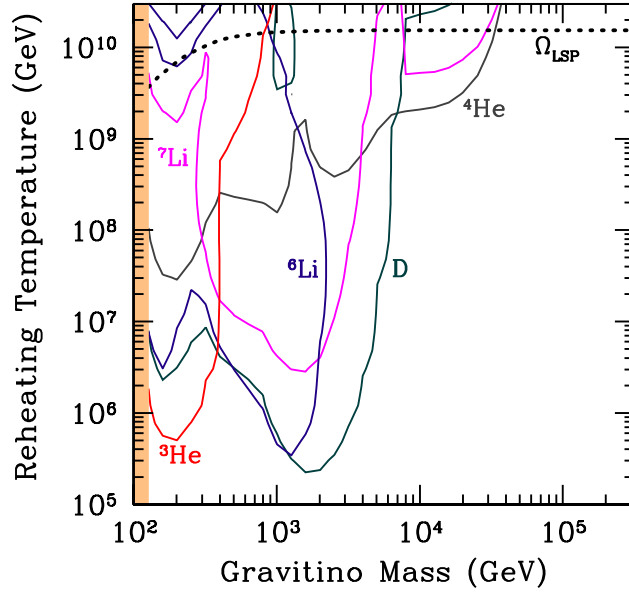


Figure 2: BBN constraints for the Case 1 at 95 % C.L. Each solid line shows upper bound on the reheating temperature from D,  $^3\text{He}$ ,  $^4\text{He}$ ,  $^6\text{Li}$ , or  $^7\text{Li}$ . The dotted line is the upper bound on the reheating temperature from the overclosure of the universe.

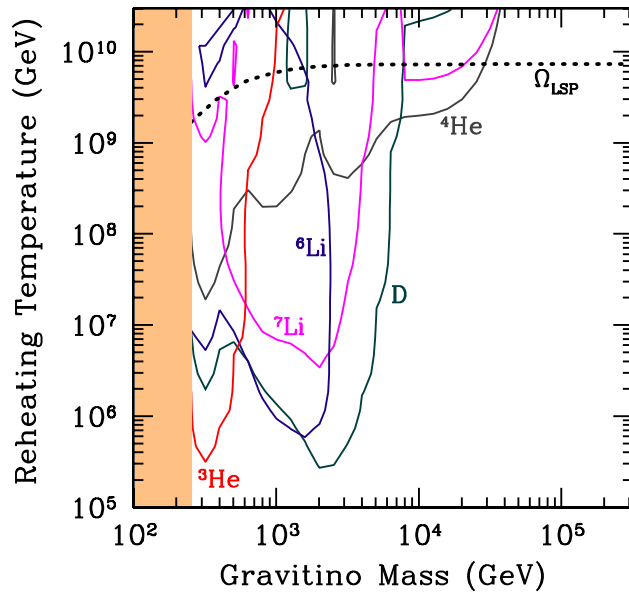


Figure 3: BBN constraints for the Case 2.

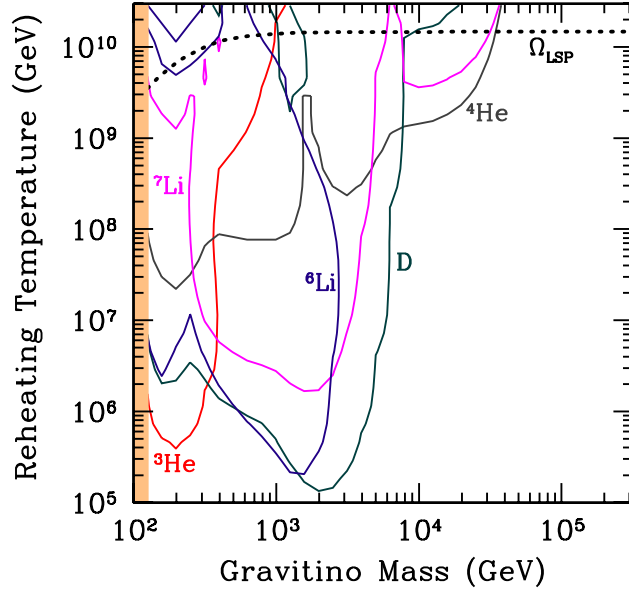


Figure 4: BBN constraints for the Case 3.

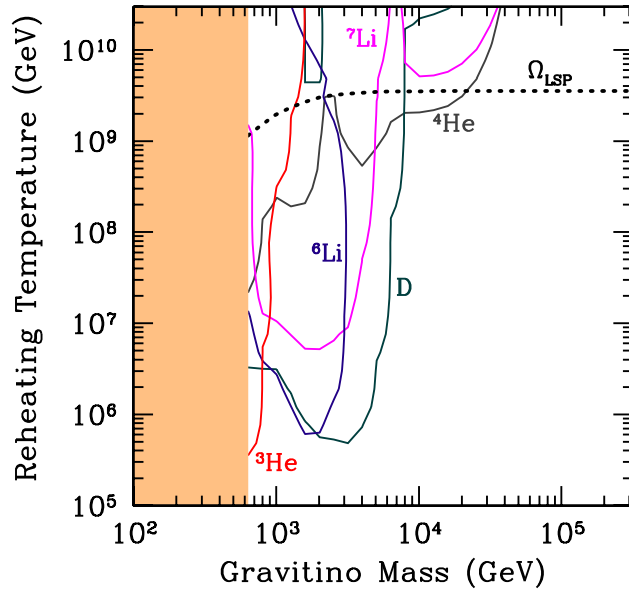


Figure 5: BBN constraints for the Case 4.

$m_{3/2}$	Case 1	Case 2	Case 3	Case 4
300 GeV	$1 \times 10^6$ ( ${}^3\text{He}$ )	$4 \times 10^5$ ( ${}^3\text{He}$ )	$1 \times 10^6$ ( ${}^3\text{He}$ )	–
1 TeV	$5 \times 10^5$ ( ${}^6\text{Li}$ )	$9 \times 10^5$ ( ${}^6\text{Li}$ )	$3 \times 10^5$ ( ${}^6\text{Li}$ )	$3 \times 10^6$ ( ${}^6\text{Li}$ )
3 TeV	$5 \times 10^5$ (D)	$4 \times 10^5$ (D)	$2 \times 10^5$ (D)	$5 \times 10^5$ (D)
10 TeV	$2 \times 10^9$ ( ${}^4\text{He}$ )	$2 \times 10^9$ ( ${}^4\text{He}$ )	$2 \times 10^9$ ( ${}^4\text{He}$ )	$2 \times 10^9$ ( ${}^4\text{He}$ )
30 TeV	$9 \times 10^9$ ( ${}^4\text{He}$ )	$8 \times 10^9$ ( ${}^4\text{He}$ )	$7 \times 10^9$ ( ${}^4\text{He}$ )	$8 \times 10^9$ ( ${}^4\text{He}$ )

Table 2: Upper bound on the reheating temperature (in units of GeV) from BBN for Cases 1 – 4. The light element which gives the most stringent bound is indicated in the parenthesis.

produced by the decay of the gravitino. Since the decay of the gravitino occurs after the freeze-out epoch of the lightest neutralino, the LSP produced by the gravitino decay survives until today. Thus, in this case, we also obtain the upper bound on the reheating temperature from the overclosure of the universe. The lightest neutralino has two origins; one is thermal relic and the other is non-thermal one from the gravitino decay. However, since the density of the thermal relic strongly depends on the MSSM parameters, we do not take into account its effect in the calculation of the density parameter. Then, the density parameter of the LSP is proportional to  $Y_{3/2}$  and is given by

$$\Omega_{\text{LSP}} h^2 \simeq 2.8 \times 10^{10} \times Y_{3/2} \left( \frac{m_{\chi_1^0}}{100 \text{ GeV}} \right), \quad (3.8)$$

where  $m_{\chi_1^0}$  is the mass of the lightest neutralino (i.e., the LSP) which is given in Table 1 for each cases. We require that  $\Omega_{\text{LSP}} h^2$  be smaller than the observed dark matter density:  $\Omega_{\text{LSP}} h^2 < 0.118$  (95 % C.L.) [22], and derive upper bound on the reheating temperature. The bound is shown in the dotted line in the figures. As one can see, the constraint from the relic density of the LSP is less severe than those from BBN unless the gravitino mass is extremely large.

In summary, when the gravitino mass is close the mass of the LSP, the most stringent bound is from the overproduction of  ${}^3\text{He}$ , resulting in the upper bound of  $O(10^{5-6} \text{ GeV})$ . When  $m_{3/2}$  is around a few TeV, the hadro-dissociation processes become most effective and the severest bound is from D or  ${}^6\text{Li}$ . With higher gravitino mass, the constraint is drastically relaxed since the gravitino lifetime becomes shorter. In particular, when the gravitino mass is larger than  $\sim 30 \text{ TeV}$  or so, the reheating temperature can be as high as  $\sim 10^{10} \text{ GeV}$ .

## 4 Stable Gravitino

### 4.1 General remarks

Next, we consider the case where gravitino is the LSP and hence is stable. In this case, the MSSM-LSP becomes unstable. We assume that the MSSM-LSP is the NLSP and that it

decays only into gravitino and standard-model particle(s). Then, the lifetime of the MSSM-LSP may become longer than 1 sec. If so, the decay products of the MSSM-LSP induce dissociation processes and change the light-element abundances. Since the lifetime of the NLSP in this case is approximately proportional to  $m_{3/2}^2$ , the scenario is constrained from BBN unless the gravitino mass is small enough. Importantly, the lifetime of the NLSP as well as the spectra of charged particles (including hadrons) produced by the NLSP decay are strongly dependent on what the NLSP is, so are the BBN constraints. Thus, in the following, we discuss several possible cases separately.

## 4.2 Case with neutralino NLSP

First, we consider the case where the NLSP is the lightest neutralino  $\chi_1^0$ . Even in this case, in fact, properties of the NLSP depends on MSSM parameters since the lightest neutralino is a linear combination of Bino  $\tilde{B}$ , neutral Wino  $\tilde{W}^0$ , and Higgsinos:

$$\chi_1^0 \equiv U_{\tilde{B}} \tilde{B} + U_{\tilde{W}} \tilde{W}^0 + U_{\tilde{H}_u} \tilde{H}_u^0 + U_{\tilde{H}_d} \tilde{H}_d^0, \quad (4.1)$$

where  $\tilde{H}_u^0$  and  $\tilde{H}_d^0$  are up- and down-type Higgsinos, respectively. To make our discussion simple, we mostly consider the case that the lightest neutralino is Bino-like (i.e.,  $U_{\tilde{B}} \simeq 1$  and  $U_{\tilde{W}} \simeq U_{\tilde{H}_u} \simeq U_{\tilde{H}_d} \simeq 0$ ). Notice that the scenarios with Bino-like lightest neutralino is realized easily. In particular, if gaugino masses obey the GUT relation, the Bino mass becomes lighter than Wino and gluino masses. In addition, assuming radiative electro-weak symmetry breaking, the Higgsino mass  $\mu_H$  becomes larger than  $M_1$  in large fraction of the parameter space [54]. With those conditions, the lightest neutralino becomes Bino-like.

If  $\chi_1^0 \simeq \tilde{B}$ , the relevant decay processes of the NLSP is  $\tilde{B} \rightarrow \psi_\mu \gamma$  and  $\tilde{B} \rightarrow \psi_\mu f \bar{f}$ , where  $\psi_\mu$  and  $f$  denote gravitino and standard-model fermions, respectively. (See Fig. 6.) Notice that the second process is mediated by virtual and on-shell  $Z$ -boson as well as virtual photon and hence, in our procedure, the decay process  $\tilde{B} \rightarrow \psi_\mu Z$  is taken into account in the process  $\tilde{B} \rightarrow \psi_\mu f \bar{f}$ . We calculate the decay rate of these processes as well as the energy spectra of the final-state particles, in particular, those of partons and electro-magnetic particles. Total decay rate of Bino-like neutralino, whose mass is  $m_{\tilde{B}} \simeq M_1$ , is well approximated by

$$\tau_{\tilde{B}}^{-1} \simeq \Gamma(\tilde{B} \rightarrow \psi_\mu \gamma) + \Gamma(\tilde{B} \rightarrow \psi_\mu Z), \quad (4.2)$$

where [55]

$$\Gamma(\tilde{B} \rightarrow \psi_\mu \gamma) = \frac{\cos^2 \theta_W}{48\pi M_*^2} \frac{m_{\tilde{B}}^5}{m_{3/2}^2} (1 - x_{3/2}^2)^3 (1 + 3x_{3/2}^2), \quad (4.3)$$

$$\begin{aligned} \Gamma(\tilde{B} \rightarrow \psi_\mu Z) &= \frac{\sin^2 \theta_W \beta_{\tilde{B} \rightarrow \psi_\mu Z}}{48\pi M_*^2} \frac{m_{\tilde{B}}^5}{m_{3/2}^2} \left[ (1 - x_{3/2}^2)^2 (1 + 3x_{3/2}^2) \right. \\ &\quad \left. - x_Z^2 \left\{ 3 + x_{3/2}^3 (-12 + x_{3/2}) + x_Z^4 - x_Z^2 (3 - x_{3/2}^2) \right\} \right], \end{aligned} \quad (4.4)$$

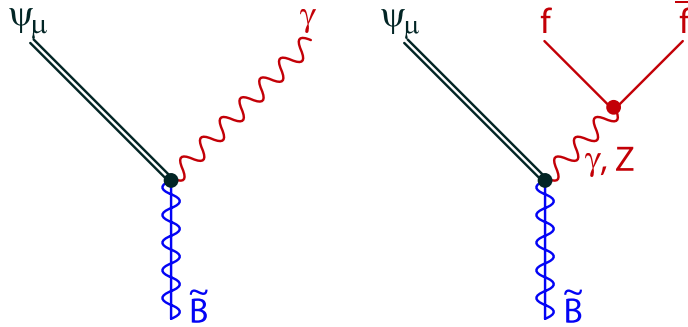


Figure 6: Feynman diagrams relevant for the decay processes of Bino-like neutralino.

with  $\theta_W$  being the Weinberg angle,  $x_{3/2} \equiv m_{3/2}/m_{\tilde{B}}$ , and  $x_Z \equiv m_Z/m_{\tilde{B}}$ . In addition, for  $m_{\tilde{B}} > m_{3/2} + m_Z$ ,

$$\beta_{\tilde{B} \rightarrow \psi_\mu Z} \equiv \left[ 1 - 2(x_{3/2}^2 + x_Z^2) + (x_{3/2}^2 - x_Z^2)^2 \right]^{1/2}, \quad (4.5)$$

while  $\beta_{\tilde{B} \rightarrow \psi_\mu Z} = 0$  otherwise.

As well as the decay rate and the energy spectra of decay products, it is also necessary to obtain the primordial abundance of the lightest neutralino in deriving the BBN constraints. The primordial abundance is determined at the time of its freeze-out if there is no entropy production after freeze out, and is strongly dependent on MSSM parameters. In our study, instead of performing a precise calculation of the primordial abundance assuming a detailed model, we first adopt approximated formulas to derive constraints. Following [55], for the abundance in the bulk region, we use

$$Y_{\tilde{B}} = 4 \times 10^{-12} \times \left( \frac{m_{\tilde{B}}}{100 \text{ GeV}} \right) \quad : \text{ bulk}, \quad (4.6)$$

while, for that in the focus-point and co-annihilation regions, we use

$$Y_{\tilde{B}} = 9 \times 10^{-13} \times \left( \frac{m_{\tilde{B}}}{100 \text{ GeV}} \right) \quad : \text{ focus / co-annihilation}. \quad (4.7)$$

Constraints on the  $m_{3/2}$  vs.  $m_{\tilde{B}}$  plane with the relic abundance given in Eqs. (4.6) and (4.7) are shown in Figs. 7 and 8, respectively. The most stringent constraint is from the overproduction of D and  ${}^4\text{He}$ ; overproduction of D is due to the hadro-dissociation of  ${}^4\text{He}$  produced by the SBBN reactions, while that of  ${}^4\text{He}$  is due to the  $p \leftrightarrow n$  conversion. Comparing Figs. 7 and 8, we can see that the constraints from the overproduction of D on the  $m_{3/2}$  vs.  $m_{\tilde{B}}$  plane are not so sensitive to  $Y_{\tilde{B}}$ . This is because the upper bound on the primordial abundance of  $\tilde{B}$  from the overproduction of D significantly changes with a slight change of the lifetime. (See Figs. 9 and 10.) On the contrary, constraint from  ${}^4\text{He}$  is sensitive to  $Y_{\tilde{B}}$ ; in the focus-point/co-annihilation case where  $Y_{\tilde{B}}$  is relatively small, constraint from  ${}^4\text{He}$  is not

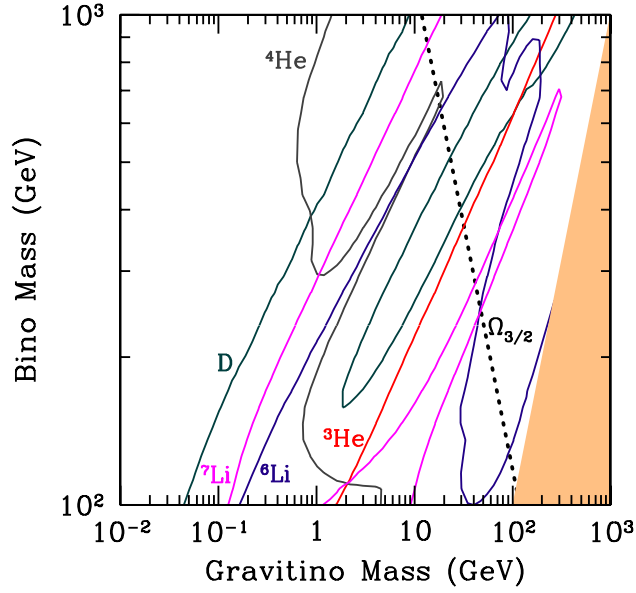


Figure 7: BBN constraints for the Bino-NLSP scenario with the abundance given in Eq. (4.6). In the shaded region, gravitino becomes heavier than the lightest neutralino and hence is not the LSP. The region with small gravitino mass is allowed.

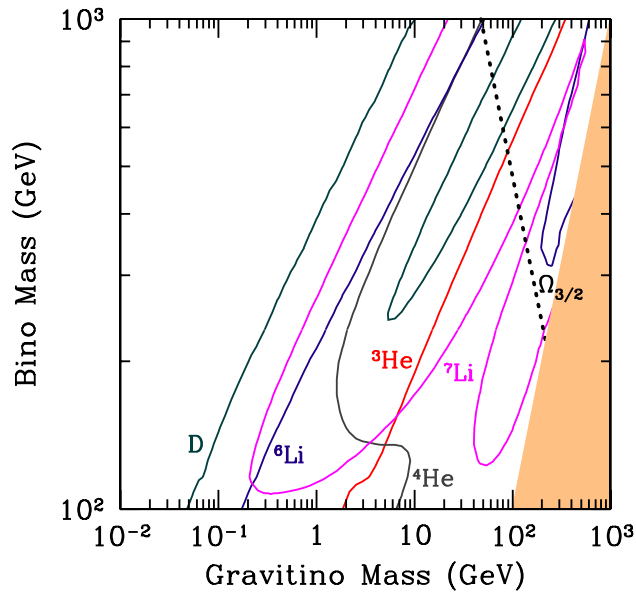


Figure 8: Same as Fig. 7, except for the abundance given in Eq. (4.7).



important while, in the bulk case,  ${}^4\text{He}$  is too much produced when the Bino mass becomes large.

Next, we treat  $Y_{\tilde{B}}$  as a free parameter and derive BBN constraints on  $m_{3/2}$  vs.  $m_{\tilde{B}}Y_{\tilde{B}}$  plane. The results are shown in Figs. 9 and 10 for  $m_{\tilde{B}} = 100$  GeV and  $m_{\tilde{B}} = 300$  GeV, respectively. When the gravitino mass is close to  $m_{\tilde{B}}$ , the lifetime of the lightest neutralino becomes relatively long. In such a case, the most stringent bound on  $Y_{\tilde{B}}$  is from the overproduction of  ${}^3\text{He}$  due to the photo-dissociation of  ${}^4\text{He}$ . On the contrary, with smaller gravitino mass, hadro-dissociation or  $p \leftrightarrow n$  conversion becomes more important than the photo-dissociation. In addition, if the gravitino mass is small enough,  $\tau_{\tilde{B}}$  becomes shorter than  $\sim 1$  sec and, in such a case, decay of the lightest neutralino becomes harmless to the BBN scenario.

So far, we have considered the case where the lightest neutralino is well approximated by the Bino. We also considered the case where the lightest neutralino has sizable Higgsino components. We derived constraints for the case  $U_{\tilde{H}_u} \simeq U_{\tilde{H}_d} \simeq 0.1$ , and found that the constraints are almost unchanged compared to the pure-Bino case.

### 4.3 Case with stau NLSP

Next, we consider the case where the NLSP is charged slepton. The basic procedure to derive constraints is explained in [14]. Here, we concentrate on the case where the NLSP is stau  $\tilde{\tau}$ , since, in some models of supersymmetry breaking, like gauge-mediation model [56] and mSUGRA model, one of the stau becomes lighter than other sleptons because of the renormalization group effects.<sup>#5</sup>

In considering long-lived stau it is crucial to take account of the bound state effect which significantly change BBN reaction rates, in particular, production rate of  ${}^6\text{Li}$  [20, 39, 57, 11, 58, 59, 43]. In the previous study by three of the present authors [14], the number density of ( ${}^4\text{He}\tilde{\tau}^-$ ) bound state was obtained with the use of Saha equation [60]. After the study, there have been several works which calculate the number density of bound state by solving the Boltzmann equation, which gives more accurate estimate [42, 59, 43]. In our current study, we also solve the full Boltzmann equation to evaluate the number density of bound-state taking effect of bound-state ( $\text{H}\tilde{\tau}^-$ ) into account.<sup>#6</sup>

The Boltzmann equations that govern the evolution of the number densities  $n_4$  and  $n_1$  of the bound states ( ${}^4\text{He}\tilde{\tau}^-$ ) and ( $\text{H}\tilde{\tau}^-$ ) are

$$\frac{dn_4}{dt} = -3Hn_4 - \Gamma_{\tilde{\tau}}n_4 + \langle\sigma_{r4}v\rangle \left[ (n_{{}^4\text{He}} - n_4)n_{\tilde{\tau}^-} - \left(\frac{m_{{}^4\text{He}}m_{\tilde{\tau}}T}{2\pi m_4}\right)^{3/2} e^{-E_{b4}/T} n_4 \right], \quad (4.8)$$

$$\frac{dn_1}{dt} = -3Hn_1 - \Gamma_{\tilde{\tau}}n_1 + \langle\sigma_{r1}v\rangle \left[ (n_p - n_1)n_{\tilde{\tau}^-} - \left(\frac{m_p m_{\tilde{\tau}} T}{2\pi m_1}\right)^{3/2} e^{-E_{b1}/T} n_1 \right], \quad (4.9)$$

<sup>#5</sup>We have checked that the constraints are almost unchanged when the NLSP is selectron or smuon.

<sup>#6</sup>See also various attempts to tackle this  ${}^6\text{Li}$  problem [52, 61, 40, 41, 62, 44] and a possibility of non-standard  ${}^9\text{Be}$  production [63] in the catalyzed BBN induced by the stau.

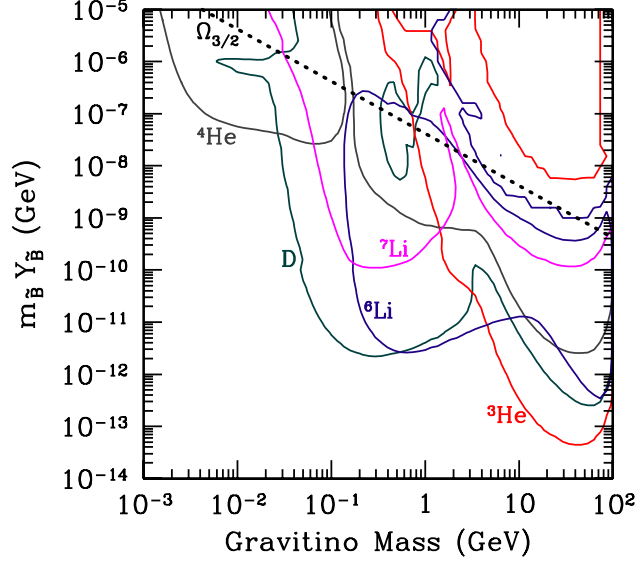


Figure 9: BBN constraints for the Bino-NLSP scenario on the  $m_{3/2}$  vs.  $m_{\tilde{B}}Y_{\tilde{B}}$  plane. The Bino mass is taken to be 100 GeV.

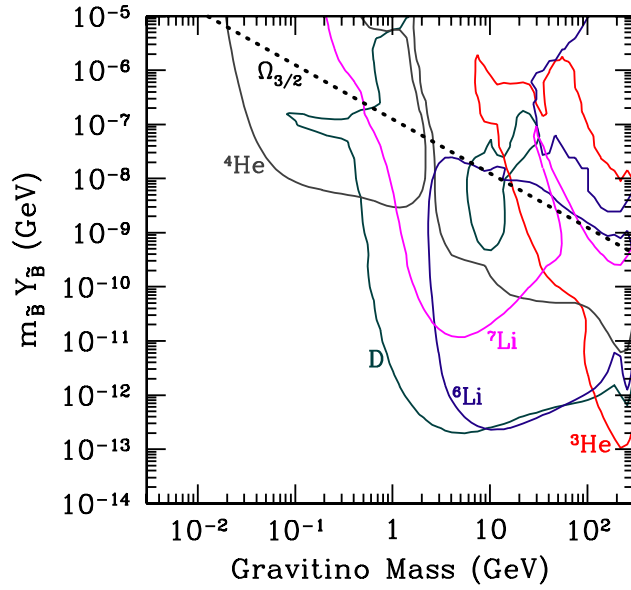


Figure 10: Same as Fig. 9, except for  $m_{\tilde{B}} = 300$  GeV.

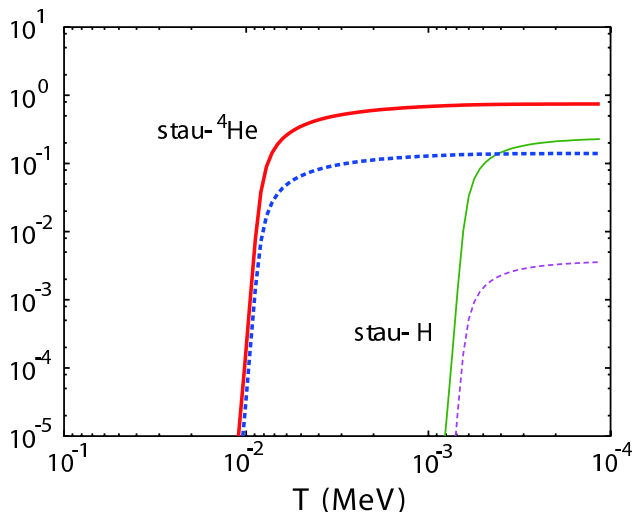


Figure 11: Time evolution of fractions of  $\tilde{\tau}^-$  which form bound-states ( ${}^4\text{He}\tilde{\tau}^-$ ) (thick solid curve) and ( $\text{H}\tilde{\tau}^-$ ) (thin solid curve). We also show  $n_4/n_{4\text{He}}$  (thick dashed curve) and  $n_1/n_p$  (thin dashed curve). We take  $Y_{\tilde{\tau}} = 2 \times 10^{-12}$ ,  $m_{\tilde{\tau}} = 1$  TeV and  $\Gamma_{\tilde{\tau}} = 0$ .

where  $n_{\tilde{\tau}^-}$  is the number density of the free negative charged stau,  $\Gamma_{\tilde{\tau}}$  is the decay rate of stau,  $E_{b4} \simeq 337.33$  keV and  $E_{b1} \simeq 24.97$  keV are the binding energies of ( ${}^4\text{He}\tilde{\tau}^-$ ) and ( $\text{H}\tilde{\tau}^-$ ) [58], and  $n_{4\text{He}}$  and  $n_p$  are the number densities of  ${}^4\text{He}$  and proton including both free and bound states. Furthermore,  $m_4 = m_{4\text{He}} + m_{\tilde{\tau}} - E_{b4}$  and  $m_1 = m_p + m_{\tilde{\tau}} - E_{b1}$ , and the thermally averaged recombination cross sections for  ${}^4\text{He}$  and  $p$  bound-states are given by [39]

$$\langle \sigma_{r4} v \rangle \simeq 98.46 \frac{\alpha E_{b4}}{m_{4\text{He}}^2 \sqrt{m_{4\text{He}} T}}, \quad (4.10)$$

$$\langle \sigma_{r1} v \rangle \simeq 24.62 \frac{\alpha E_{b1}}{m_p^2 \sqrt{m_p T}}. \quad (4.11)$$

An example of the evolution of the abundances of the bound-states ( ${}^4\text{He}\tilde{\tau}^-$ ) and ( $\text{H}\tilde{\tau}^-$ ) are shown in Fig. 11.

First, we use the following thermal relic abundance of  $\tilde{\tau}$  [64]:

$$Y_{\tilde{\tau}} \simeq 7 \times 10^{-14} \times \left( \frac{m_{\tilde{\tau}}}{100 \text{ GeV}} \right), \quad (4.12)$$

and derive constraints on  $m_{3/2}$  vs.  $m_{\tilde{\tau}}$  plane. The result is shown in Fig. 12. As one can see, the most stringent bound is from the overproduction of  ${}^6\text{Li}$ , which is due to the catalyzed process. On the contrary, the bound from D is less severe compared to the Bino-NLSP case. This is because, when the stau is the NLSP, the hadronic branching ratio is several orders

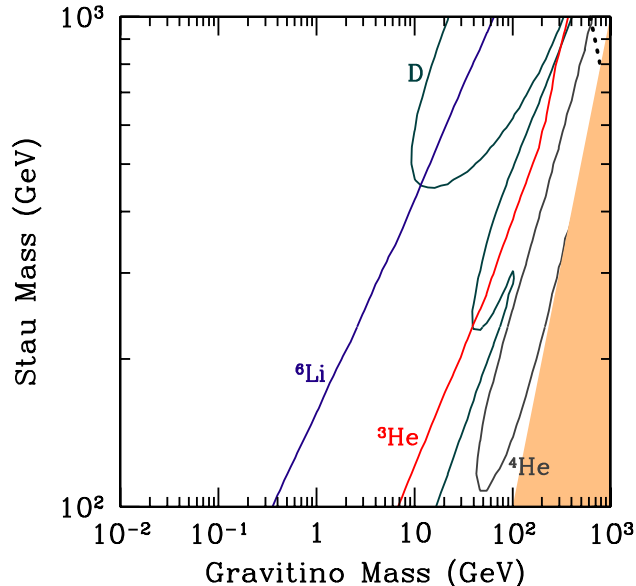


Figure 12: BBN constraints for the stau-NLSP scenario with the thermal abundance given in Eq. (4.12).

of magnitude smaller than that in the Bino NLSP case, and hence the hadro-dissociation processes are suppressed.

We also treat the primordial abundance as a free parameter and derive upper bound on  $Y_{\tilde{\tau}}$ . The results for  $m_{\tilde{\tau}} = 100$  GeV and 300 GeV are shown in Figs. 13 and 14, respectively.<sup>#7</sup> The  ${}^4\text{He}$ -constraint for smaller gravitino mass comes from the  $p \leftrightarrow n$  conversion induced by the charged pions which are mainly produced by the decay of tau lepton [14]. On the other hand, the D-constraint comes from the destruction due to energetic baryons produced by the four-body decay. Thus, for the stau case a simple scaling of the constraints on Bino by using the hadronic branching ratio does not work.

As we mentioned, in the present study, we have solved the full Boltzmann equation to calculate the number density of the  $({}^4\text{He}\tilde{\tau}^-)$  and  $(\text{H}\tilde{\tau}^-)$  bound states. Then, as discussed in [59, 43], the number density of  $({}^4\text{He}\tilde{\tau}^-)$  is reduced compared to the result with Saha equation, resulting in weaker constraint than the previous study. However, the upper bound on  $Y_{\tilde{\tau}}$  from the overproduction of  ${}^6\text{Li}$  is increased by the factor 3 or so. Thus, we conclude that the previous study with Saha equation provided a reasonable estimation of the upper bound on  $Y_{\tilde{\tau}}$ . Notice that, concerning the constraints on the  $m_{3/2}$  vs.  $m_{\tilde{\tau}}$  plane, the change

<sup>#7</sup>The bound states with singly-charged nuclei such as  $(\text{H}\tilde{\tau}^-)$ ,  $(\text{D}\tilde{\tau}^-)$  or  $(\text{T}\tilde{\tau}^-)$  may shield coulomb field of the nuclei completely and significantly enhance the further reaction rates for these nuclei. These non-standard processes might totally have reduced the  ${}^6\text{Li}$ ,  ${}^7\text{Li}$  and  ${}^7\text{Be}$  abundances [39, 42, 43]. However, the Bohr radius of those bound states are larger than the typical size of the nuclei (or the square-root of the cross sections). Then the multi-body problem might be important for reactions and could not have been understood well. Therefore, we did not include those effects in the current study.

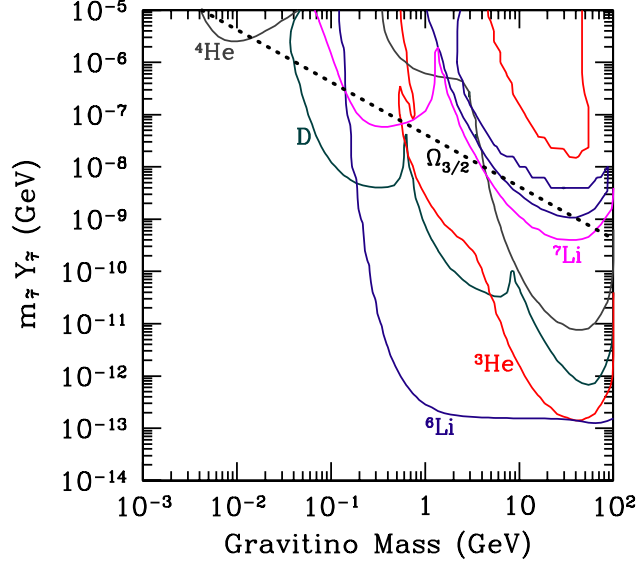


Figure 13: BBN constraints for the stau-NLSP scenario on the  $m_{3/2}$  vs.  $m_{\tilde{\tau}} Y_{\tilde{\tau}}$  plane. The stau mass is taken to be 100 GeV.

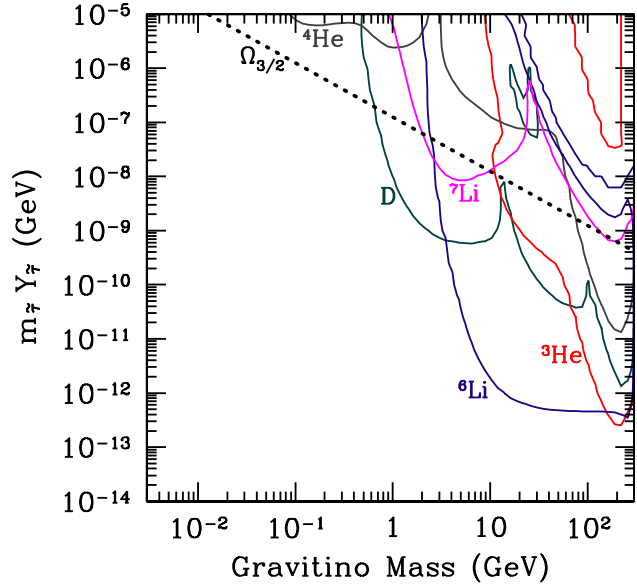


Figure 14: Same as Fig. 13, except for  $m_{\tilde{\tau}} = 300$  GeV.

is negligible.<sup>#8</sup>

## 4.4 Case with sneutrino NLSP

Finally we study the case with sneutrino LSP. Although such a scenario is not conventional, it is possible to realize sneutrino MSSM-LSP in some gravity mediation scenario. In this paper we update the constraint obtained in [13] using the most recent observational data.

The yield variable for thermally produced sneutrino is estimated as [64]

$$Y_{\tilde{\nu}} \simeq 2 \times 10^{-14} \times \left( \frac{m_{\tilde{\nu}}}{100 \text{ GeV}} \right), \quad (4.13)$$

where  $m_{\tilde{\nu}}$  is the sneutrino mass. With this yield variable, we derive the constraint on  $m_{3/2}$  vs.  $m_{\tilde{\nu}}$  plane and the result is shown in Fig. 15. The resultant constraint is almost same as that in [13] since the most stringent constraints come from overproduction of D and  ${}^6\text{Li}$  whose observational abundances have not changed very much. As expected, the constraints are much weaker than the Bino- or stau-NLSP cases because the sneutrino dominantly decays into particles whose interactions are weak;  $\tilde{\nu} \rightarrow \psi_{\mu}\nu$ . The BBN constraints are from four-body decay modes  $\tilde{\nu} \rightarrow \psi_{\mu}\nu f\bar{f}$ , which have very small branching ratios.

We also treat the primordial abundance as a free parameter and derive upper bound on  $Y_{\tilde{\nu}}$ . The result for  $m_{\tilde{\nu}} = 300 \text{ GeV}$  is shown in Fig. 16. Compared to the previous study [13], it is seen that the constraint from  ${}^4\text{He}$  is slightly milder due to the larger observational constraint on  $Y_{\text{p}}$  than that adopted in [13].

## 5 Conclusions and Discussion

In this paper we have obtained the improved BBN constraints on both unstable and stable gravitino cases. We have taken into account recent theoretical and observational progresses in the study of BBN constraints on long-lived unstable particles.

In the unstable gravitino case, we have included effects of the longitudinal component which was not considered in the previous studies, which have led to a more stringent upper-bound on the reheating temperature for gravitino with relatively small mass. The upper bound on the reheating temperature strongly depends on the gravitino mass and has been summarized in Table 2 for the MSSM parameters used in our analysis. We can see that the upper bound has mild dependence on the mass spectrum of the MSSM particles, and that the bound becomes almost independent of the MSSM parameters when the gravitino becomes much heavier than the MSSM superparticles. Our results give very stringent constraint on the scenario of thermal leptogenesis [65] which requires the reheating temperature higher than  $O(10^9 \text{ GeV})$  [66, 67].

---

<sup>#8</sup>Ref. [40] suggested a mechanism to reduce the  ${}^7\text{Li}$  ( ${}^7\text{Be}$ ) abundance through  $({}^7\text{Be}\tilde{\tau}^-) + p \rightarrow ({}^8\text{B}\tilde{\tau}^-) + \gamma$  which is effective for  $Y_{\tilde{\tau}} \gtrsim 10^{-11}$  and  $\tau_{\tilde{\tau}} \lesssim 10^3 \text{ sec}$ . Because we have adopted the conservative observational  ${}^7\text{Li}$  abundance which agrees with the SBBN prediction, this mechanism does not change our results.

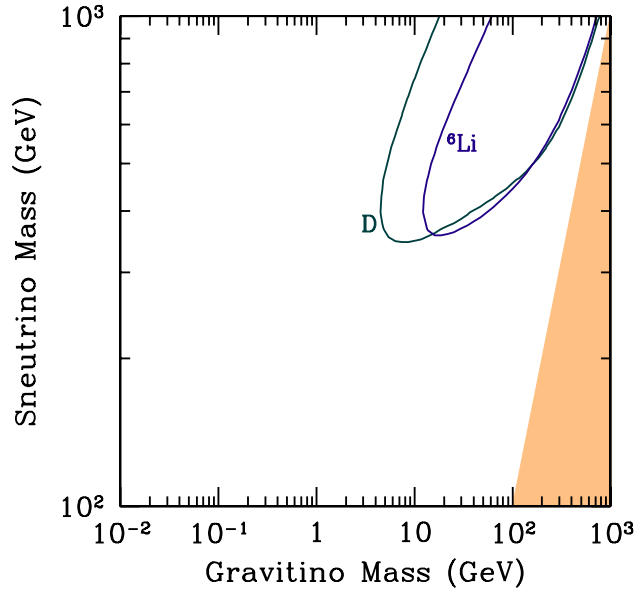


Figure 15: BBN constraints for the sneutrino-NLSP scenario with the thermal abundance given in Eq. (4.13).

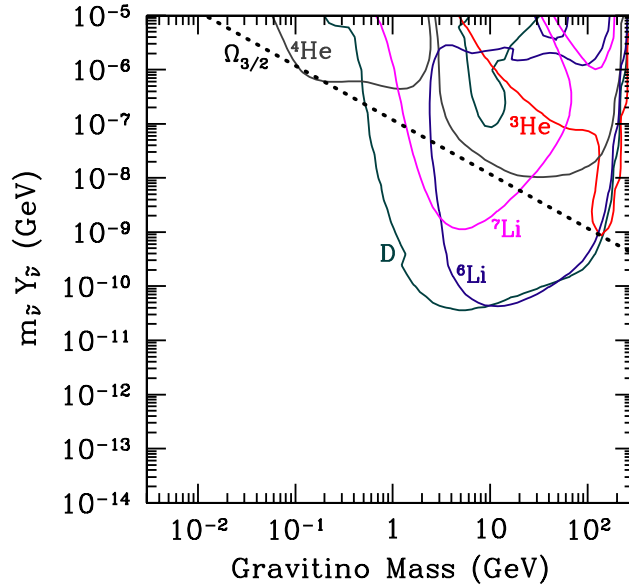


Figure 16: BBN constraints for the snu-NLSP scenario on the  $m_{3/2}$  vs.  $m_{\tilde{\nu}} Y_{\tilde{\nu}}$  plane. The sneutrino mass is taken to be 300 GeV.

When the gravitino is the LSP and stable, the constraints depend on which superparticle is the NLSP. We have considered Bino, stau and sneutrino as NLSP and obtained constraints on their properties. Among these possibilities, the hadronic branching ratio becomes largest when the Bino is the NLSP, for which the constraints from the hadro-dissociation processes are the most stringent. For the case of stau as NLSP, we have estimated the effects of bound-state of stau with  ${}^4\text{He}$  accurately by solving the Boltzmann equation describing evolution of the bound-state abundance. However, the bound from the catalyzed production process of  ${}^6\text{Li}$  is almost unchanged with the previous study where Saha equation was used, and the overproduction of  ${}^6\text{Li}$  gives stringent bound on the primordial abundance of stau. In these two cases, the constraints are so stringent that the gravitino mass larger than  $\sim 10$  GeV is excluded when the mass of the MSSM-LSP (i.e., Bino or stau) is lighter than 1 TeV. If the sneutrino is the NLSP, on the contrary, BBN constraints become drastically weaker since the sneutrino mainly decays into very weakly interacting particles, i.e., gravitino and neutrino. However, in any case, our results provide severe constraint on some scenario of gravitino dark matter. Indeed, as we can see in Figs. 7, 8, 12, and 15, the constraints from BBN are severer than that from the overclosure of the universe. This fact implies that the abundance of the gravitino produced by the decay of the MSSM-LSP cannot be sufficient to realize the gravitino dark matter if the thermal relic abundance of the MSSM-LSP is assumed. Thus, in order to realize the gravitino dark matter, most of the gravitino should be produced by, for example, the scattering processes of thermal particles at the time of the reheating after inflation [9] or by the decay of scalar condensation [49, 50].

*Acknowledgements:* This work was supported in part by PPARC grant PP/D000394/1, EU grants MRTN-CT-2004-503369 and MRTN-CT-2006-035863, and the European Union through the Marie Curie Research and Training Network “UniverseNet” (K.K.). This work was also supported in part by the Grant-in-Aid for Scientific Research from the Ministry of Education, Science, Sports, and Culture of Japan, No 14102004 (M.K.) and No. 19540255 (T.M.), and JSPS-AF Japan-Finland Bilateral Core Program (M.K.).

## References

- [1] S. Weinberg, Phys. Rev. Lett. **48**, 1303 (1982).
- [2] J. R. Ellis, J. E. Kim and D. V. Nanopoulos, Phys. Lett. B **145**, 181 (1984); M. Y. Khlopov and A. D. Linde, Phys. Lett. B **138** (1984) 265; D. Lindley, Astrophys. J. **294**, 1 (1985); J. R. Ellis, D. V. Nanopoulos and S. Sarkar, Nucl. Phys. B **259**, 175 (1985); R. Juszkiewicz, J. Silk and A. Stebbins, Phys. Lett. B **158** (1985) 463.
- [3] J. R. Ellis *et al.*, Nucl. Phys. B **373**, 399 (1992); M. Kawasaki and T. Moroi, Prog. Theor. Phys. **93**, 879 (1995); E. Holtmann, M. Kawasaki, K. Kohri and T. Moroi, Phys. Rev. D **60**, 023506 (1999); K. Jedamzik, Phys. Rev. Lett. **84**, 3248 (2000); M. Kawasaki,



- K. Kohri and T. Moroi, Phys. Rev. D **63**, 103502 (2001); R. H. Cyburt, J. R. Ellis, B. D. Fields and K. A. Olive, Phys. Rev. D **67**, 103521 (2003).
- [4] M. Kawasaki and T. Moroi, Astrophys. J. **452**, 506 (1995).
- [5] M. Kawasaki, K. Kohri and T. Moroi, Phys. Lett. B **625**, 7 (2005).
- [6] M. Kawasaki, K. Kohri and T. Moroi, Phys. Rev. D **71**, 083502 (2005).
- [7] K. Kohri, T. Moroi and A. Yotsuyanagi, Phys. Rev. D **73**, 123511 (2006).
- [8] J. R. Ellis, K. A. Olive and E. Vangioni, Phys. Lett. B **619**, 30 (2005).
- [9] T. Moroi, H. Murayama and M. Yamaguchi, Phys. Lett. B **303**, 289 (1993).
- [10] J. L. Feng, A. Rajaraman and F. Takayama, Phys. Rev. Lett. **91**, 011302 (2003); Phys. Rev. D **68**, 063504 (2003); J. R. Ellis, K. A. Olive, Y. Santoso and V. C. Spanos, Phys. Lett. B **588**, 7 (2004); J. L. Feng, S. Su and F. Takayama, Phys. Rev. D **70**, 063514 (2004); Phys. Rev. D **70**, 075019 (2004); D. G. Cerdeno et al, JCAP **0606**, 005 (2006); F. D. Steffen, JCAP **0609**, 001 (2006); J. L. Diaz-Cruz et al, JHEP **0705**, 003 (2007).
- [11] R. H. Cyburt *et al.*, JCAP **0611**, 014 (2006).
- [12] K. Jedamzik, K. Y. Choi, L. Roszkowski and R. Ruiz de Austri, JCAP **0607**, 007 (2006).
- [13] T. Kanzaki, M. Kawasaki, K. Kohri and T. Moroi, Phys. Rev. D **75**, 025011 (2007).
- [14] M. Kawasaki, K. Kohri and T. Moroi, Phys. Lett. B **649**, 436 (2007).
- [15] M. Kusakabe, T. Kajino and G. J. Mathews, Phys. Rev. D **74**, 023526 (2006).
- [16] M. H. Reno and D. Seckel, Phys. Rev. D **37**, 3441 (1988); K. Kohri, Phys. Rev. D **64**, 043515 (2001).
- [17] K. Jedamzik, Phys. Rev. D **74**, 103509 (2006).
- [18] S. Dimopoulos, R. Esmailzadeh, L. J. Hall and G. D. Starkman, Astrophys. J. **330**, 545 (1988).
- [19] S. Dimopoulos, R. Esmailzadeh, L. J. Hall and G. D. Starkman, Nucl. Phys. B **311**, 699 (1989).
- [20] M. Pospelov, Phys. Rev. Lett. **98**, 231301 (2007).
- [21] L. Kawano, FERMILAB-PUB-92-004-A, (1992).
- [22] D. N. Spergel *et al.* [WMAP Collaboration], Astrophys. J. Suppl. **170**, 377 (2007).
- [23] F. E. Paige, S. D. Protopopescu, H. Baer and X. Tata, arXiv:hep-ph/0312045.

- [24] T. Sjostrand *et al.*, Comput. Phys. Commun. **135**, 238 (2001).
- [25] K. Jedamzik, Phys. Rev. D **70**, 063524 (2004).
- [26] D. Cumberbatch *et al.*, Phys. Rev. D **76**, 123005 (2007).
- [27] J. M. O’Meara *et al.*, Astrophys. J. **649**, L61 (2006)
- [28] G. Sigl, K. Jedamzik, D. N. Schramm and V. S. Berezinsky, Phys. Rev. D **52**, 6682 (1995).
- [29] J. Geiss and G. Gloeckler, Space Science Reviews **106**, 3 (2003).
- [30] Y. I. Izotov, T. X. Thuan and G. Stasinska, arXiv:astro-ph/0702072.
- [31] M. Fukugita and M. Kawasaki, Astrophys. J. **646**, 691 (2006).
- [32] M. Peimbert, V. Luridiana and A. Peimbert, arXiv:astro-ph/0701580.
- [33] P. Bonifacio *et al.*, arXiv:astro-ph/0610245.
- [34] S.G. Ryan *et al.*, Astrophys. J. Lett. **530**, L57 (2000).
- [35] J. Melendez and I. Ramirez, Astrophys. J. **615**, L33 (2004).
- [36] M. H. Pinsonneault, G. Steigman, T. P. Walker and V. K. Narayanan, Astrophys. J. **574**, 398 (2002).
- [37] A. Coc *et al.*, Astrophys. J. **600**, 544 (2004); C. Angulo *et al.*, Astrophys. J. **630**, L105 (2005); A. J. Korn *et al.*, Nature **442**, 657 (2006).
- [38] K. Ichikawa and M. Kawasaki, Phys. Rev. D **69**, 123506 (2004); K. Ichikawa, M. Kawasaki and F. Takahashi, Phys. Lett. B **597**, 1 (2004).
- [39] K. Kohri and F. Takayama, Phys. Rev. D **76**, 063507 (2007).
- [40] C. Bird, K. Koopmans and M. Pospelov, arXiv:hep-ph/0703096.
- [41] T. Jittoh *et al.*, Phys. Rev. D **76**, 125023 (2007).
- [42] K. Jedamzik, arXiv:0707.2070 [astro-ph].
- [43] K. Jedamzik, arXiv:0710.5153 [hep-ph].
- [44] M. Kusakabe *et al.*, Phys. Rev. D **76**, 121302 (2007); arXiv:0711.3858 [astro-ph].
- [45] W. M. Yao *et al.* [Particle Data Group], J. Phys. G **33**, 1 (2006).
- [46] B. Fields and S. Sarkar, arXiv:astro-ph/0601514.

- [47] M. Asplund *et al.*, *Astrophys. J.* **644**, 229 (2006).
- [48] M. H. Pinsonneault, T. P. Walker, G. Steigman and V. K. Narayanan, *Astrophys. J.* **527**, 180 (1999).
- [49] M. Endo, K. Hamaguchi and F. Takahashi, *Phys. Rev. Lett.* **96**, 211301 (2006); S. Nakamura and M. Yamaguchi, *Phys. Lett. B* **638**, 389 (2006); M. Dine, R. Kitano, A. Morisse and Y. Shirman, *Phys. Rev. D* **73**, 123518 (2006); M. Endo, K. Hamaguchi and F. Takahashi, *Phys. Rev. D* **74**, 023531 (2006).
- [50] M. Kawasaki, F. Takahashi and T. T. Yanagida, *Phys. Lett. B* **638**, 8 (2006); *Phys. Rev. D* **74**, 043519 (2006); M. Endo, F. Takahashi and T. T. Yanagida, *Phys. Rev. D* **76**, 083509 (2007); *Phys. Lett. B* **658**, 236 (2008).
- [51] M. Bolz, A. Brandenburg and W. Buchmuller, *Nucl. Phys. B* **606**, 518 (2001) [Erratum-*ibid.* **790**, 336 (2008)].
- [52] J. Pradler and F. D. Steffen, *Phys. Lett. B* **648**, 224 (2007).
- [53] A. Ferrantelli, arXiv:0712.2171 [hep-ph].
- [54] See, for example, M. Drees, R. Godbole and P. Roy, “Theory and phenomenology of sparticles: An account of four-dimensional N=1 supersymmetry in high energy physics,” *Hackensack, USA: World Scientific* (2004).
- [55] J. L. Feng, S. Su and F. Takayama, in [10].
- [56] M. Dine, A. E. Nelson and Y. Shirman, *Phys. Rev. D* **51** (1995) 1362; M. Dine, A. E. Nelson, Y. Nir and Y. Shirman, *Phys. Rev. D* **53** (1996) 2658.
- [57] M. Kaplinghat and A. Rajaraman, *Phys. Rev. D* **74**, 103004 (2006); F. D. Steffen, arXiv:hep-ph/0611027.
- [58] K. Hamaguchi *et al.*, arXiv:hep-ph/0702274.
- [59] J. Pradler and F. D. Steffen, arXiv:0710.2213 [hep-ph].
- [60] See, for example, E. W. Kolb and M. S. Turner, “The Early universe,” *Front. Phys.* **69**, 1 (1990).
- [61] W. Buchmuller *et al.*, *JHEP* **0703**, 037 (2007).
- [62] S. Kasuya and F. Takahashi, *JCAP* **0711**, 019 (2007); F. Takayama, arXiv:0704.2785 [hep-ph]; N. Okada and O. Seto, arXiv:0710.0449 [hep-ph]; J. Kersten and K. Schmidt-Hoberg, arXiv:0710.4528 [hep-ph]; E. J. Chun *et al.*, *JHEP* **0803**, 061 (2008).
- [63] M. Pospelov, arXiv:0712.0647 [hep-ph].

- [64] M. Fujii, M. Ibe and T. Yanagida, Phys. Lett. B **579**, 6 (2004).
- [65] M. Fukugita and T. Yanagida, Phys. Lett. B **174**, 45 (1986).
- [66] W. Buchmuller, P. Di Bari and M. Plumacher, Annals Phys. **315**, 305 (2005).
- [67] G. F. Giudice *et al.*, Nucl. Phys. B **685**, 89 (2004).